Annals of Work Exposures and Health, 2023, **67**, 1088–1098
https://doi.org/10.1093/annweh/wxad048
Advance access publication 4 September 2023
Original Article

Non-ionizing radiation modeling to predict ambient irradiance in work areas at an indoor cannabis farm

Maximilian Chmielinski[1], Michael G. Yost[1], Martin Cohen[1], Mehlika Inanici[2] and Christopher D. Simpson[1,*]

[1]Department of Environmental and Occupational Health Sciences, University of Washington, 3980 15th Ave NE, Seattle, WA 98195, United States
[2]Department of Architecture, University of Washington, 208 Gould Hall, 3950 University Way NE, Seattle, WA 98105, United States

[*]Corresponding author: Department of Environmental and Occupational Health Sciences, University of Washington, Seattle, WA, United States. Email: simpson1@uw.edu

Abstract

Agricultural workers frequently experience potentially hazardous exposure to non-ionizing radiation from both solar and artificial sources, and measurement of this exposure can be expensive and impractical for large populations. This project develops and evaluates a vegetative radiative transfer model (VRTM) to predict irradiance in a grow room of an indoor cannabis farm. The model uses morphological characteristics of the crop, manufacturer provided lamp emissions data, and dimensional measurements of the grow room and cannabis hedgerows to predict irradiance. A linear regression comparing model predictions with the measurements taken by a visible light spectroradiometer had slopes within 23% of unity and R^2 values above 0.88 for visible (400–700 nm), blue (400–500 nm), green (500–600 nm), and red (600–700 nm) wavelength bands. The excellent agreement between the model and the measured irradiance in the cannabis farm grow room supports the potential of using VRTMs to predict irradiance and worker exposure in agricultural settings. Because there is no mechanistic difference between visible and other non-ionizing wavelengths of radiation in regards to mechanisms of radiative transfer, the model developed herein for visible wavelengths of radiation should be generalizable to other radiation bands including infrared and ultraviolet radiation.

Key words: horticulture; indoor; Marijuana; non-ionizing radiation; radiative transfer; UV

What's Important About This Paper?'

Exposure to ultraviolet radiation and blue light poses both acute and chronic hazards to human health. This study estimates visible light conditions using a predictive model built on an open-source radiative transfer model, and validates the accuracy of the model predictions through comparison with measurements taken by a spectroradiometer. The model predictions had excellent agreement with measurements and model implementation does not experience the cost and spectral limitations inherent in radiometry.

Introduction

Considerable research has linked ultraviolet (UV) radiation and blue light exposure to various health hazards, including skin damage (Ichihashi et al. 2003), eye damage (Pitts and Tredici 1971), circadian rhythm disruption (Hatori et al. 2017), immune system suppression (IARC 2012), and various types of cancer (IARC 2012). Outdoor agricultural worker exposure to UV radiation has been widely studied (Glanz et al. 2007) and exposures in the outdoor farmer population

Received: April 16, 2023. Accepted: August 7, 2023.

have been directly linked to negative health outcomes such as an increased risk of melanoma (Togawa et al. 2021) and lip cancer (Acquavella et al. 1998). In contrast, only a few studies have documented indoor farm worker exposure to UV radiation from artificial lights (Chmielinski et al. 2018). No research has yet studied the health outcomes of indoor farm worker radiation exposure, a gap due, in part, to the lack of exposure research on this topic. This research gap is becoming more important because of the increasing prevalence of supplemental lighting use across horticultural farms in the United States, evidenced by the 46% increase in the size of the grow lamp industry between 2016 and 2021 (Grandview Research 2022). This growth is driven, in part, by new research showing the benefits of supplemental lighting on crop yield benefits (Lu and Mitchell 2016) and the rapidly decreasing costs of agricultural lamps (Morrow 2008).

Direct measurements of personal exposure are often viewed as the gold standard for exposure assessment. However, collecting personal exposure measurements can be expensive, and may not be practical for large populations. In the absence of direct measurements, exposure models can be used to make predictions of personal exposure. Predictive exposure models can provide additional benefits, including (i) identifying potentially hazardous exposures a priori, for example during design of a facility or process and (ii) estimating the effect on worker exposure of changes in work processes or facilities. This project develops a model for predicting worker exposure to non-ionizing radiation—as a surrogate for exposure to UV radiation—in an indoor cannabis farm. Model performance is then evaluated via comparison with measurements of visible light irradiance in a cannabis farm in Washington State made using a visible light spectroradiometer.

Methods

Dimensional measurements

A 3D representation of a cannabis grow room was created as an input for the VRTM simulation model. To create this representation, measurements of the location and dimensions of all lamps, hedgerows, and walls in the grow room using a DISTO D2 laser distance meter (Leica Geosystems; Heerbrugg, Switzerland). The DISTO D2 device had published measurement error of ±1.5 mm, calibrated at distances of 0.64, 2.47, and 7.84 m.

The grow room had a length, width, and height of 13.1 m × 7.62 m × 2.57 m and contained 48 Vividrgo V2 (model ID: VGROHB 600W P26 MVOLT CLR PND BLK) lamps (Illumitex, Austin, TX). The room contained 24 wheeled hedgerow platforms, each of which held 4 cannabis plants contained within individual 5-gallon pots. The platforms had a width of 0.68 m and a length of 2.75 m, and the canopies on the platforms had dense vegetation between a height of 1.18 m and 1.66 m (see Fig. 1A,B). At the time of measurement, the plants were in the late stages of their flowering cycle, close to harvest. The Vividgro V2 lamps hung above the hedgerow platforms in parallel at a height of 2.16 m. The room ceiling had a height of 2.57 m.

Optical measurement

Instrumentation

Visible light measurements were taken using the Ocean Insight (Orlando, FL, USA) Flame-S spectroradiometer with a QP450-1-XSR fiber connecting a CC-3-UV-S cosine corrector optical inlet. The manufacturer provided a radiometric calibration performed using a DH-3P-CAL deuterium and tungsten halogen source traceable to the National Institute of Science and Technology. The calibration stated that the device wavelength uncertainty was <0.0001% and the irradiance measurement error ranged from 8.0% at 400 nm to 2.8% at 700 nm. The device was controlled by an in-house designed controller based on the Arduino Due platform allowing a technician to initiate an optical measurement with the push of a button (Chmielinski et al. 2022). Irradiance measurements were recorded at integration times that resulted in 80% of pixel saturation at the peak wavelength. The optical inlet to the spectrometer was attached to a flexible arm that allowed precise control of the inlet position and orientation.

Measurement of emissions from an isolated lamp

Emissions from a single isolated lamp in the grow room were measured in order to verify the data contained in the manufacturer-provided Illuminating Engineering Society (IES) LM-79 report describing lamp emission intensity and angular distribution (BACL 2015). The technician isolated a single lamp in plant row 21 near the center of the room using blackout curtains (Amazon Essentials, Seattle, WA), and the lid of an HDX 27 gallon storage tote. Spectroradiometric measurements were obtained as described in Supplementary Appendix 2, section 2.c.v at a distance of 0.94 m from the center of the lamp. All 48 lamps in the room remained active during these measurements.

Procedure for irradiance measurements in a grow room

Irradiance was measured at multiple locations within the grow room for subsequent evaluation of the performance of the VRTM model. Each optical measurement consisted of a positional and optical component. The laser distance meter was used to take horizontal

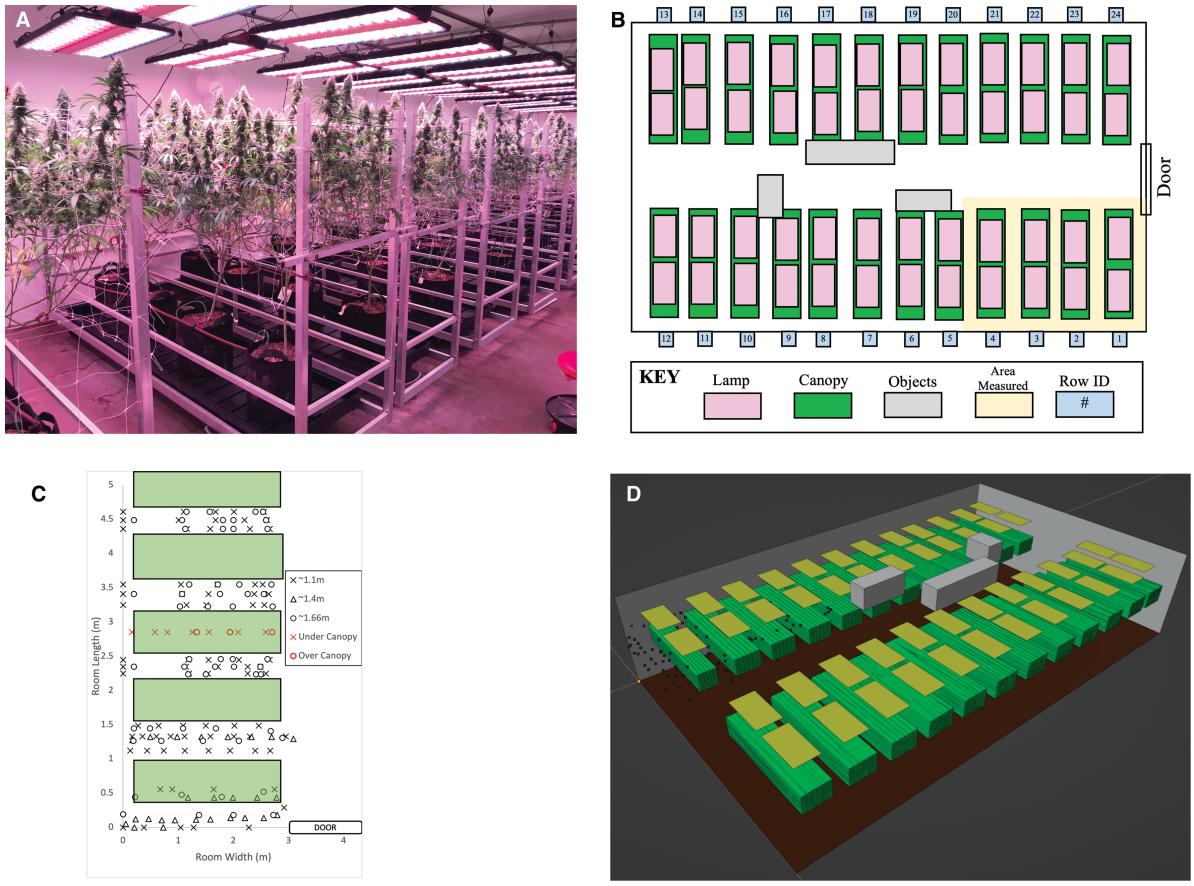

Fig. 1. Various representations of the grow room including (A) a photograph taken in the room showing the wheeled rectangular hedgerow platforms and Vividgro V2 lamps hanging in parallel above, (B) a to scale top view of the grow room with "Objects" representing room HVAC and equipment, (C) a top view of the measured area in the grow room with measurement locations designated by marker symbols, (D) the virtual 3D space used for validation of the VTRM model with the 3D space consisting of the lamps (yellow), canopies (green), walls (grey), floor (brown), room objects (gray), and a ceiling (not visible) and the real-world locations of the spectroradiometric measurements represented as tiny black dots.

and vertical positional measurements of the optical inlet at each measurement location.

On the first day of data collection, measurements were taken at heights slightly above (~1.66 m from the floor), at the midpoint (~1.4 m), and slightly below the plant canopy (~1.1 m) in the aisles between plant platform "1" and the wall and between plant platforms "1" and "2" (). If the technician perceived a risk of contact between the optical inlet and vegetation, the height of the optical inlet was adjusted slightly (± < 0.05 m).

On the second day of data collection, the measurements were taken at heights of ~1.1 m and ~1.66 m in the aisles in between plant platforms labeled as "2," "3," "4," and "5" (Fig. 1C). In the interest of time and to minimize crop disturbance, the technician decided to stop measurement about three fourths of the way down the aisles. Overall, a total of 57 measurements were collected at ~1.66 m, 25 measurements at ~1.4 m, and 78 measurements at ~1.1 m. Additionally, the technician took 2 sets of measurements directly below (n = 7) and directly above (n = 3) the plant canopy on plant platform "3" at heights of 0.87 and 1.81 m, respectively.

Measurement of cannabis leaf transmittance and reflectance

Information on the optical properties of cannabis leaves was required as inputs for the VRTM model. Hence, cannabis leaf transmittance and reflectance was measured on 20 cannabis leaves, as described in Supplementary Appendix 3. These measurements were then used to calculate the absorptivity of the cannabis leaves in the visible wavelength range (400–700 nm).

The computed average adaxial absorptivity values were red (600–700 nm) 0.950, green (500–600 nm) 0.937, and blue (400–500 nm) 0.969, respectively.

Radiation modeling

Vegetation radiative transfer models (VRTM) consist of methods to derive plant canopy optical properties from plant morphology and to characterize radiation propagation through those canopy representations (Goudriaan 1977, 1988; Campbell and Norman 2000; Xu and Wei 2019). This project uses a VRTM based on an open-source backwards ray tracing simulation engine named the Radiance Lighting Simulation and Rendering System (*Radiance*, version 5.4)—an open-source lighting simulation software package (Ward 1994)—to predict irradiance at selected locations in a single grow room at an indoor cannabis farm in Bellingham, WA.

Radiance uses backwards ray-tracing to solve an equation that outputs the radiance emitted, transmitted, or reflected at surfaces within a 3D space. The environment consists of a 3D space filled with 2D surface representations of real-world objects, called primitives, to which a user may assign optical properties. Simulations using *Radiance* generate rays from nodes in the 3D space (Ward and Shakespeare 1998). A node generates a user specified number of rays that propagate outward from the center of the node. Each node has an orientation and generates rays in that hemispherical direction with uneven hemispherical distribution. Peak ray generation density occurs close to the orientation of the node (Mardaljevic 2011). The rays generated by the node do not interact with that node, other nodes, or other rays in the 3D space.

The model predicts irradiance in a 3D virtual representation of a real-world grow room. This 3D representation represents the geometry of real-world objects within the grow room using the *Radiance* primitive named "polygon" and the optical properties of the real-world objects using a variety of other "material" primitives. The details of *Radiance* and VRTM structure may be found in Supplementary Appendices 1 and 2, respectively.

Virtual representation of real-world grow room

Information on lamp emissions and angular distribution is required as an input for the VRTM model. Geometric measurements of the grow room were used to define a virtual 3D space that contained representations for each lamp in the room (n = 48), polygons representing the walls, ceiling, and floor (n = 6), polygons representing HVAC components in the room (n = 18), polygons representing the hedgerows (n = 5304; 24 hedgerows × 221 primitives per hedgerow), and nodes that correspond to the real world measurement locations (Fig. 1D).

Lamps

The Vividgro V2 lamp manufacturer provides a LM-79 report that details both the emission's intensity and the angular profile. These data were translated into "light" and "brightdata" *Radiance* material primitives, characterizing the lamp emissions in the 3D space. The resulting red, green, and blue (RGB) emission intensities passed into the "light" material primitive in W/m^2*sr are 74.06, 12.60, and 13.00. A 2-dimensional table of angular adjustment factors and a lamp area correction were passed to the "brightdata" material primitive. Supplementary Appendix 2.c.v details the translation of the LM-79 report data to the RGB emission intensities and spatial adjustment factors.

Wall, floor, and object reflectance

The polygons representing the walls, floor, and ceiling were assigned plastic material primitives with RGB diffuse reflectance values set to match those found in literature for the materials observed at the cannabis farm. Materials assigned to walls and ceiling received reflectance parameters matching that of conventional white paint (Dornelles et al. 2010) and the material assigned to the floor received reflectance parameters matching that of 21 MPa concrete (Lee et al. 2012). The diffuse reflection values for the walls and ceiling were 0.95, 0.95, and 0.78 and for the floor were 0.36, 0.34, and 0.29 for the 600–700 nm, 500–600 nm, and 400–500 nm wavelength bands, respectively.

Optical properties of cannabis canopy

Leaf absorptivity, canopy leaf area index (L_I, the one-sided green leaf area per unit ground surface area), and 2 parameters related to the leaf area density (L_D, the ratio of the one-sided leaf area to a volume within the canopy) are needed to calculate optical extinction of the cannabis canopy. The 2 parameters related to L_D are the horizontal modifier u, and the fraction of canopy height at peak leaf density v. Since 3 of the 4 parameters could not be measured directly, the Nelder Mead algorithm implemented in python (Olsson and Nelson 1975) was used to fit values for L_I, u, and v. Supplementary Appendix 2 provides further details on the 4 canopy parameters and Supplementary Appendix 4 provides an overview of the of the Nelder Mead algorithm and fitting process.

Simulation implementation and statistical analysis

Python 3.10.3 (Python Software Foundation 2023) provided the scripting environment for the VRTM. All executed *Radiance* simulations used the settings listed in Table 1-1 in Supplementary Appendix 1. The algorithm ran for fifty iterations and the results section presents

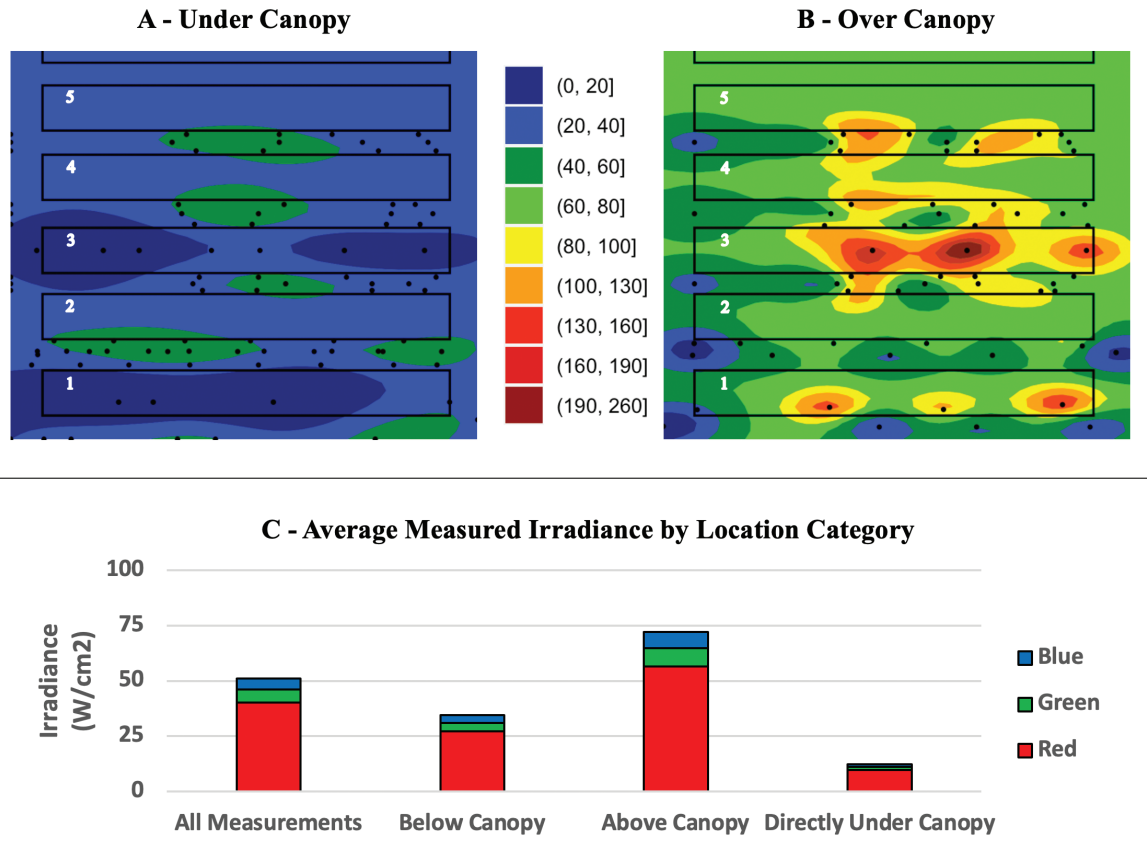

Fig. 2. Visualizations of measured irradiance that include heatmaps of the irradiance measurements taken at heights (A) under the canopy and (B) above the canopy using a common scale in W/m^2 and (C) a bar chart of the averages of the irradiance measurements in W/m^2, grouped by spectral band and measurement height category.

tabulations and summary statistics for the convergent parameter values and the resulting RMSE and R2 values. Heatmaps of the total irradiance measurements were generated using the "autoKrige" function of the automap library to generate the "geom_contour_filled" function of the ggplot2 library within R 4.1.3 (R Core Team 2022).

Summary statistics were computed for the predictions at the same locations as that of the irradiance measurements. The relationship between the measured and predicted values was investigated using paired *t*-tests as well as linear regression. Summary statistics, *t*-tests, and linear regressions were run in Microsoft Excel for Mac (ver. 16.71) (Microsoft Corporation 2023). Bubble plots were generated using R 4.1.3 to visualize the percent error between the measured and predicted values for locations below and above the canopy.

Results

Isolated lamp measurements

The lamp emissions generated from isolated lamp measurements were 96.1 (red), 13.85 (green), and 12.4 (blue) W/m^2*sr, respectively. The summation of the 3 wavelength bands yields a measured visible lamp emission of 122.3 W/m^2*sr.

Grow room measurements

Figure 2A and B shows heatmaps of the measurements taken under the canopy at a height of ~1.1 m and above the canopy at a height of ~1.66 m. Figure 2C shows a bar chart of mean irradiance measurements in the grow room, grouped by measurement height and color coded by wavelength bound. Table 5-1 in Supplementary Appendix 5 presents summary statistics of the irradiance measurements visualized in the referenced figures.

The minimum, maximum, mean, and standard deviation of the above canopy measurements for all wavelength bands exceeded those generated from the measurements taken below the canopy by at least a factor of 2. The heatmap constructed from measurements taken below the canopy indicates that measurements away from the center of an aisle between hedgerows have comparatively lower irradiance

values than those taken in the aisle center. The second heatmap shows the inverse; the locations with the highest measurement values are those at the edge of the aisles or directly above each row of cannabis plants. The locations above hedgerow "3" are directly underneath the lamps.

Parameter fitting

Table 1 presents values for the optical properties of the cannabis canopy fit by the fifty executions of the Nelder Mead algorithm (run on a VRTM that uses the lamps constructed from the manufacturer LM-79 report), together with R^2 and RSME values for the VRTM model fit.

The VRTM converged to the upper boundary for L_l 25 of 50 times, the upper boundary of the v modifier 37 times, the lower boundary of v a single time and the lower boundary of the u modifier 11 times. The algorithm never converged to the lower boundary of L_l or the upper boundary of the u modifier. The minimum and maximum RMSE and R^2 differed by 4.85 and 0.003, respectively.

Irradiance predictions

Table 5-2 in Supplementary Appendix 5 presents summary statistics of the irradiance predictions, grouped by wavelength bound and by measurement height, for the predictions generated by the model run with the best RMSE.

Figure 3 presents scatter plots and linear regressions of the measurements vs predictions for the full visible light range as well as the RGB wavelength bands for the parameters associated with the model run that had the lowest RMSE.

The linear regressions show strong linear correlation between the measured and predicted values across all wavelength bands ($R^2 > 0.88$). The regression results show that the predictions underestimate the total and red irradiance and overestimate the green and blue irradiance.

Figure 4 shows heatmaps and bubble plots of the predicted irradiances and percent error between the measured and predicted values.

The minimum and maximum percent error over all measurements was −84% to 185%. The mean of the percent error was 6.9% (SD = 38.18%).

Discussion

Isolated lamp measurements

The computed emission values for the isolated lamp differ from those listed in the LM-79 report by +29% in the red, +10% in the green, −5% in the blue, and +23% in the visible. The field team did encounter problems isolating a single lamp. It is possible that emissions from the surrounding lamps during measurement of emissions from the single isolated lamp may have resulted in overestimation of the measured emissions in the red and green bands for the isolated lamp. Emissions were only measured from a single lamp, and although all lamps in the room were the same make and model, research has shown that lamp aging can cause variable spectral degradation among identical lamps (Ke et al. 2018). Notably, and as discussed below, excellent R^2 values (>0.88) were obtained between measured and predicted values of irradiance in the grow room for models using either lamp emissions based on the manufacturer's LM-79 file, or models that used the measured emissions from the isolated lamp.

Table 1. Cannabis canopy parameters fit by Nelder Mead algorithm (run on a VRTM that uses the lamps constructed from the manufacturer LM-79 report), summary statistics for the RMSE and R^2 values from the runs, and the fit parameters corresponding to the VRTM with the lowest RMSE and the highest R^2.

Parameter	L_l[a]	Horizontal L_D[b] Modifier (u)	Fraction of Height at Peak L_D (v)	RMSE (W/m^2)	R^2
Min	10.3	0.01	0.01	142.2	0.888
Max	15.0	6.10	1.00	147.1	0.892
Median	15.0	0.82	1.00	142.6	0.891
Mean	14.0	1.09	0.96	142.8	0.891
SD	1.57	1.15	0.15	0.8	0.001
Run with lowest RMSE	15.0	1.30	1.00	142.2	0.891
Run with best R^2	15.0	2.73	1.00	142.6	0.892

[a]L_l = Leaf area index
[b]L_d = Leaf area density

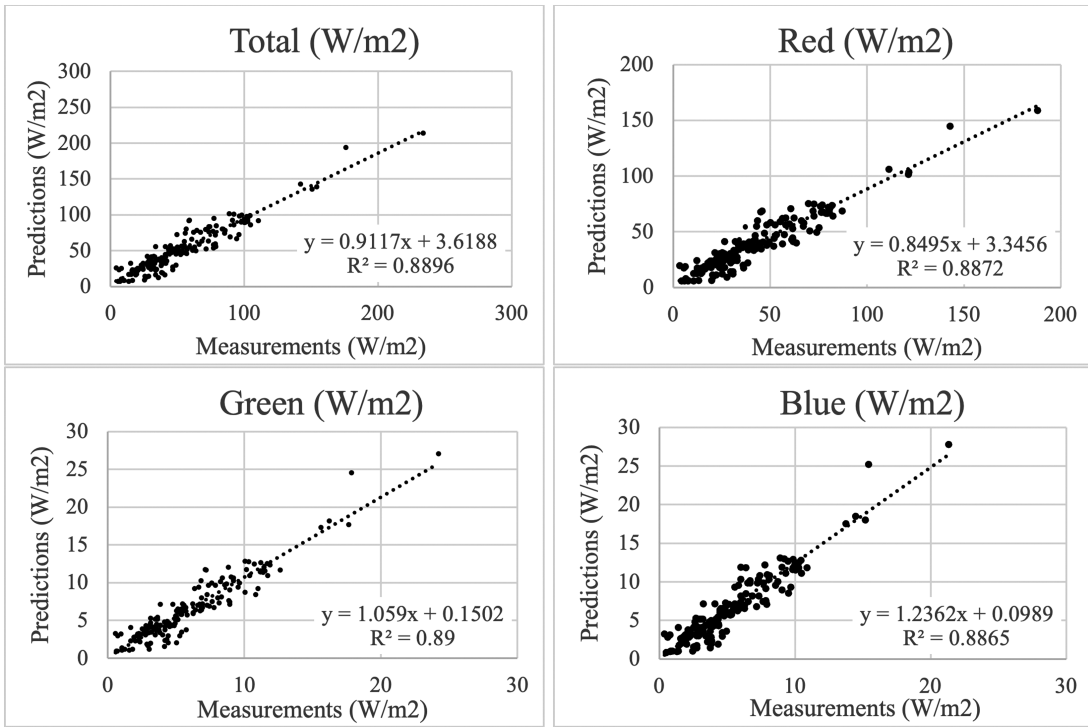

Fig. 3. Scatterplots of the measurements vs predictions for the total, red, green, and blue wavelength bands. Each plot contains the results of a linear regression.

Room irradiance measurements and modeling

The location with the largest measured irradiance was located directly under the lamp (233 W/m^2) at a height of 1.81 m, while the measurement with the smallest measured irradiance was located slightly under the canopy (4.07 W/m^2) at a height of 1.07 m. The mean irradiance of the measurements taken above the canopy is larger than those taken below the canopy. This is expected as measured irradiance should be greater when closer to the lamps.

The heatmaps of simulated irradiances (Fig. 4) share some visual similarity with the heatmaps of measured irradiances (Fig. 2). However, the measurement heatmaps contain visual discontinuities not seen in the prediction heatmap. These discontinuities probably result from spatial sparsity of measurement and use of kriging to interpolate irradiances in areas where measurements are sparse, especially in the areas proximal to left wall and hedgerows 2, 3, 4, and 5.

The large coefficient of variation (0.55) computed from the 7 measurements taken directly under the canopy indicates that the canopy does not have a uniform leaf density distribution. This non-uniformity is likely a major source of error in the model agreement with the measurements below the canopy. The large coefficient of variation (0.53) computed from the measurements taken above the canopy probably results from measurement locations overlapping or not overlapping with a lamp's cone of illumination.

The results of the linear regressions show excellent agreement between the measured and predicted irradiance. The slope of the linear regressions for the total visible and red wavelength bands were 9% and 15% below unity, indicating underestimation, while the slope of the linear regressions for the green and blue wavelength bands were 6% and 23% above unity, indicating overestimation. A potential cause of this prediction error is the manufacturer LM-79 report underestimating lamp emissions in the red wavelength band while overestimating lamp emissions in the green and blue wavelength bands. A subsequent section further details lamp influence on regression slope.

Canopy influence on predictions

Model simulations both without the canopy included in the simulation, and with opaque canopies included in the simulation, to investigate the effect of canopy extinction on model fit. The no canopy simulation predictions greatly overestimated irradiance at locations

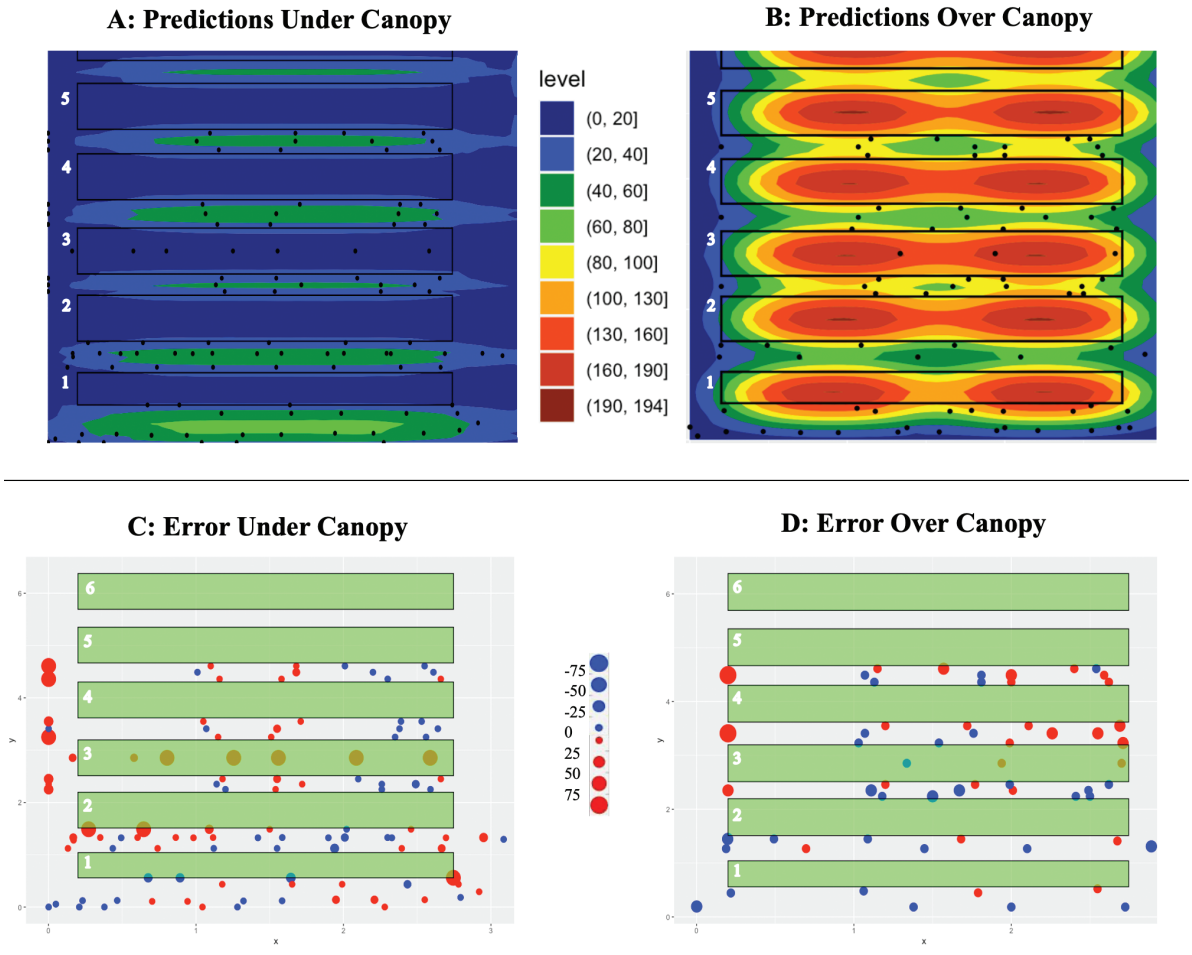

Fig. 4. The top 2 graphics show simulation predictions at nodes set at 1.1 m (A) and 1.66m (B) using a common scale in W/m^2. The bottom graphics show bubble plots of the percent error between the measurements and model predictions. Bubbles colored blue show locations where the model has underestimated the measured value. Under canopy =1.1 m (C); Over Canopy = 1.66 m (D).

below the plant canopy, resulting in poor linear regression fit ($R^2 < 0.2$). However, linear regressions using the predictions of the opaque canopy simulation had good agreement with the measurements ($R^2 > 0.87$). This performance is comparable to the base model, suggesting the real-world canopies have a large extinction effect on the lamp emissions. Supplementary Appendix 5 (Supplementary Figs 5-1 and 5-2) contains summary statistics, scatterplots, and linear regression visualizations for both simulations.

Fitted canopy parameters

All algorithm runs converged to values of L_I above 10.2, and converged to the upper boundary of 15 for 25 of the 50 runs. An L_I value of 10.2 already describes a very thick canopy, and an L_I value of 15 is in the 99th percentile of the 2653 species reported in the Global Database of Field-observed Woody Tree species (Lio and Ito 2014). The large differences between the convergent values and those published in literature casts doubt on the accuracy of the convergent L_I values.

The model runs converged to a u value of ~1.3, implying that leaf density decreases when moving away from the center of a canopy. The runs that converged to the boundary value of 0.01 had the worst RMSEs, implying that the horizontal L_D is not homogeneous throughout a canopy. This result is supported by the photo of the cannabis canopies presented in which illustrates higher leaf density toward the center of a cannabis canopy.

The runs converged to a value of v of 1, the top of the canopy. This value suggests that the canopy thickness increases when moving upwards from the bottom to the top of the plant canopy. This result is somewhat supported by the photo of the canopies

presented in Fig. 1A, which shows canopies thickening as the vertical position in the canopy increases. However, the same image shows the peak leaf area density occurring at a position below the top of the canopy, casting doubt on the accuracy of the fit value. Almost all of our measurements were collected either above or below the height of the plant canopy. The absence of measurements at heights within the plant canopy may have made it difficult to derive an accurate value of v.

Taking measurements only outside the canopies likely limited the ability of the Nelder Mead algorithm to reliably fit the canopy parameters. The decision to restrict measurement to outside the canopy was intentional and motivated by preliminary attempts that resulted in the optical inlet becoming coated with plant resin. The coating necessitated immediate cleaning with disposable optical wipes, and the potentially equipment damaging experience underpinned the decision to avoid measurement of optical conditions inside the hedgerow itself. Notably, the observation that simulating canopies as fully opaque boxes yielded a model fit essentially identical to the model using fitted parameters describing the optical properties of the canopy L_1, u and v (Fig. 3 versus Supplementary Appendix Fig. 5-2) demonstrates that the model is not especially sensitive to the values of L_1, u and v.

Effect of wall and floor reflection on irradiance predictions

Four simulations were run to investigate the influence of wall and floor reflection on simulation predictions. The 4 simulations ran on 3D spaces that (i) had the walls set to 0% diffuse reflection, (ii) had the walls set to 100% diffuse reflection, (iii) had the floor set to 0% diffuse reflection, and (iv) had the floor set to 100% diffuse reflection. Outside of the diffuse reflection change, all other 3D space properties matched that of the base model and the canopy parameters listed under best RMSE in Table 1. Linear regressions between the measurements versus predictions resulted in R^2 and slopes within 3% of those from the linear regressions are shown in Fig. 3, indicating that the wall and floor reflection have minimal effect on radiation transfer in the grow room. Table 5-4 in Supplementary Appendix 5 presents these results.

Effect of lamp emissions on irradiance predictions

A simulation using lamp geometries assigned optical properties based on our direct measurement of emissions from a single isolated lamp and canopy parameters with the lowest RMSE listed in Table 1 resulted in an RMSE of 308. This RMSE value is approximately twice that of the base VRTM.

Linear regressions between the measurements and predictions returned slopes of 1.13, 1.12, 1.18, and 1.19 and R^2 values of 0.889, 0.886, 0.890, and 0.888 for the red, green, blue, and total visible wavelength bands, respectively (See Fig. 5-3 in Supplementary Appendix 5). These slopes are approximately 10–20% above unity for all 4 wavelength bands, suggesting the measured lamp emissions overestimate the true lamp emissions. The slopes differ from the slopes listed in Fig. 3 by +31%, +11%, –4%, and +24%, respectively. These discrepancies are within ±2% of the discrepancies listed in the discussion of isolated lamp measurements that compares the measured lamp emission values with the manufacturer provided data. The proportional discrepancies indicate that the lamp emission data has a direct and proportional effect on the irradiance predictions from the VRTM model. The above notwithstanding, model performance was still excellent (R^2 values > 0.88) using emissions data from the manufacturer provided LM-79 report, which demonstrates that direct measurements of the lamp emissions was not necessary in order to implement the VRTM model.

VRTM applications to worker protection

Concerns related to worker health associated with exposure to lamp emitted UV underpin interest in using VRTMs to predict UV exposures. Although the current model was developed based on measurements of visible radiation, the underlying principles of the model are equally applicable to UV radiation. To extend this model to UV wavelengths, information on lamp emissions in the UV wavelength band would be required, together with information on cannabis leaf transmittance and reflectance in the UV band.

VRTM predictions can quickly identify existing work areas where the irradiance has an intensity sufficient to exceed a health criterion in a period shorter than that of a worker's scheduled shift in the area. The VRTM predictions provide a quantitative estimate of the degree of health criterion exceedance, and the combined awareness of location and severity can guide the implementation of administrative controls. The VRTM can be used as a prototyping environment to investigate the effectiveness of control strategies that eliminate, substitute, or otherwise barrier the optical hazard.

The current implementation of the VRTM is limited to predicting the irradiance in a work area, not estimating exposure directly. However, the VRTM's prediction capabilities may provide more accurate insights into irradiance received by workers than current dosimetry technologies allow. This is because currently

available broadband dosimeters suffer from spectral mismatch when measuring radiance with a different spectrum than that of the dosimeter's calibration spectrum. Spectral mismatch can cause errors exceeding 1000%, especially in environments where multiple optical sources exist. VRTM predictions do not suffer from spectral mismatch error, provided manufacturer lamp emissions data is accurate and available.

Future research should investigate the use of VRTMs in the design of indoor farms to prevent hazardous optical conditions prior to construction and the viability of using static or dynamic 3D representations of workers as a surrogate of dosimetry monitoring.

Conclusion

The VRTM accurately predicted irradiances in the visible wavelength band in a grow room of an indoor cannabis farm using only manufacturer provided specifications for grow lamps, simple 3D representations of grow room objects and some information on the optical properties of those objects. Linear regressions between VRTM predictions and spectroradiometric measurements for the red, green, blue, and visible wavelength bands showed strong correlation (R^2 > 0.89). Model predictions were similar when using realistic optical properties of cannabis plants compared to treating cannabis hedgerows as opaque boxes. This finding implies that cannabis hedgerows are relatively dense and strongly attenuate radiation transfer in grow rooms. The canopy density may come as a consequence of Washington State limits on a farm's square footage serving as a grow area, which encourages a high density of cannabis plants to maximize production of cannabis flower (WAC 2022).

Further research is needed to validate if the VRTM accuracy can be replicated in other indoor grow rooms and ones with thinner vegetation. The model was shown to be robust to changes in wall and floor reflectance, which indicates that wall and floor reflectance did not substantially influence radiative transfer within the room.

The use of a VRTM has several advantages over use of optical measurement devices in the context of indoor farm exposure characterization. An open-source simulation engine costs much less than the purchase, calibration, and maintenance costs of an appropriate measurement device. Use of a VRTM requires far less crop disturbance than optical measurements, and can predict irradiance at every location in the grow room in a relatively short period of time. Meanwhile, optical measurement of a small grow room with comparable spatial resolution to that of the VRTM capability will likely take days. Finally, VTRM predictions can be used to efficiently optimize design of a grow room before it is built to ensure optimal irradiance for plant growth while avoiding levels of irradiance that would be hazardous to workers in the facility.

Acknowledgments

We would additionally like to thank the cannabis business owners for providing access to their facilities. The content is solely the responsibility of the authors and does not necessarily represent the official views of the United States Centers for Disease Control or the National Institutes of Health.

Funding

This work was supported by the National Institute of Occupational Safety and Health (5 T42 OH008433) and by the National Institute of Environmental Health Sciences (P30ES007033).

Data availability

All data contained in the tables and figures of this manuscript will be made available upon reasonable request.

Conflict of interest statement

The authors declare no competing interests.

Supplementary data

Supplementary data are available at *Annals of Work Exposures and Health* online.

References

Acquavella J, Olsen G, Cole P, Ireland B, Kaneene J, Schuman S, Holden L. Cancer among farmers: a meta-analysis. *Ann Epidemiol*. 1998:8(1):64–74. https://doi.org/10.1016/s1047-2797(97)00120-8

BACL. *IES LM-79-08 Test Report for the Vividgro V2 Grow Light Model: VGROHB 600W P26 MVOLT CLR PND BLK*. Guangdong (CN): Bay Area Compliance Laboratories. 2015. https://greencreative.com/wp-content/uploads/PKS180801080-10-1-GREEN-CREATIVE-90HIDHB-850-BYP-EX39-LM-79-final.pdf (accessed 30 March 2023).

Campbell GS, Norman JM. *An Introduction to Environmental Biophysics*. 2nd ed. New York, NY: Springer; 2000. p. 247–278. https://doi.org/10.1007/978-1-4612-1626-1_15.

Chmielinski M, Ehrlich T Kaminsky L, Cohen M, Isaken T, Simpson C Measuring Worker Exposures to Bulb Generated Ultraviolet Radiation in the Cannabis Industry [Poster

Abstract]. In American Industrial Hygiene Conference and Exposition (AIHce). Philadelphia; 2018.

Chmielinski, M, Cohen M, Yost M, Simpson C. Wearable spectroradiometer for dosimetry. *Sensors*. 2022:**22**(22):8829. https://doi.org/10.3390/s22228829

Dornelles K, Roriz V, Roriz M, Caram RM. Spectral behaviour of cool paints produced in Brazil for roof paint and their impact on the thermal comfort and energy use in buildings designed for hot climates. Proceedings of conference: Adapting to change: new thinking on comfort. Cumberland Lodge, Windsor, UK, 9–11. London: Network for Comfort and Energy Use in Buildings; 2010. http://nceub.org.uk; https://doi.org/10.13140/RG.2.1.4104.8802

Glanz K, Buller DB, Saraiya M. Reducing ultraviolet radiation exposure among outdoor workers: State of the evidence and recommendations. *Environ Health*. 2007:**6**(22). https://doi.org/10.1186/1476-069X-6-22.

Goudriaan J. *Crop micrometeorology: a simulation study*. Wangeningen, The Netherlands: Wageningen University; 1977.

Goudriaan J. The bare bones of leaf-angle distribution in radiation models for canopy photosynthesis and energy exchange. *Agric For Meteorol*. 1988:**43**(2):155–169. https://doi.org/10.1016/0168-1923(88)90089-5.

Grandview Research. *Grow Light Market Analysis By Application (Indoor Farming, Vertical Farming, Commercial Greenhouse)*. San Francisco; 2022. www.grandviewresearch.com/industry-analysis/grow-light-market (Accessed 5 February 2023).

Hatori M, Gronfier C, Van Gelder RN, Bernstein PS, Carreras J, Panda S, Marks F, Sliney D, Hunt CE, Hirota T, *et al*. Global rise of potential health hazards caused by blue light-induced circadian disruption in modern aging societies. *Aging and Mechanisms of Disease*. 2017:**3**(9):1–3. https://doi.org/10.1038/s41514-017-0010-2.

IARC. A review of Human Carcinogens Part D. Radiation. In: Evaluation of carcinogenic risks to humans, editors. *IARC Working group on the Monographs on the evaluation of carcinogenic risks to humans*. Geneva, CH: International Agency for Research on Cancer; 2012:35–101.

Ichihashi M, Ueda M, Budiyanto A, Bito T, Oka M, Fukunaga M, Tsuru K, Horikawa T. UV-induced skin damage. *Toxicology*. 2003:**189**(1–2):21–39. https://doi.org/10.1016/S0300-483X(03)00150-1.

Ke H, Hao J, Tu J, Miao P, Wang C, Chen D, Yang S, Cui J. Study on the chromaticity of LED lamps given by online test during accelerated aging under thermal stress. *Optik*. 2018:**164**:510–518. https://doi.org/10.1016/j.ijleo.2018.02.120.

Lee J, Dewitt B, Lee S, Bhang K, Sim J. Analysis of concrete reflectance characteristics using spectrometer and VNIR Hyperspectral Camera. *International Archives of the Photogrammetry, Remote Sensing and Spatial Information Sciences*. 2012:127–130. https://doi.org/10.5194/isprsarchives-XXXIX-B7-127-2012

Lio A, Ito A. A global database of field-observed leaf area index in woody plant species. *Oak Ridge National Laboratory Distributed Active Archive Center*. Tennessee: Oak Ridge; 2014. http://dx.doi.org/10.3334/ORNLDAAC/1231

Lu N, Mitchell C. Supplemental lighting for greenhouse grown fruiting vegetables. In: Kozai T, Fujiwara K, Runkle ES, editors. *LED Lighting for Urban Agriculture*. Singapore: Springer Nature; 2016;219–230.

Mardaljevic J. Ambient calculation: crash course. In: *10th Annual International Radiance Workshop*. Berkeley (CA): Berkeley Lab; 2011. https://www.radiance-online.org/community/workshops/2011-berkeley-ca/presentations/day1/JM_AmbientCalculation.pdf (Accessed: 31 March 2023).

Microsoft Corporation. *Microsoft Excel Version 16.71*. Redmond (WA): Microsoft; 2023.

Morrow RC. LED lighting in horticulture. *HortScience*. 2008:**43**(7):1947–1950. https://doi.org/10.21273/HORTSCI.43.7.1947

Olsson DM, Nelson LS. The nelder-mead simplex procedure for function minimization. *Technometrics*. 1975:**17**(1):45–51. https://doi.org/10.1080/00401706.1975.10489269

Pitts DG, Tredici TJ. The effects of ultraviolet on the eye. *Am Ind Hyg Assoc J*. 1971:**32**(4):235–246. https://doi.org/10.1080/0002889718506444.

Python Software Foundation. Python 3.11.1 Documentation. 2023. https://docs.python.org/3/ (Accessed 1 January 2023).

R Core Team. R: a language and environment for statistical computing. 2022. https://www.R-project.org/ (Accessed: 1 January 2023).

Togawa K, Leon ME, Lebailly P, Beane Freeman LE, Nordby K-C, Baldi I, MacFarlane E, Shin A, Park S, Greenlee RT, *et al*. Cancer incidence in agricultural workers: findings from an international consortium of agricultural cohort studies (AGRICOH). *Environ Int*. 2021:**157**:106825. https://doi.org/10.1016/j.envint.2021.106825

Washington State Administrative Code [WAC]. Cannabis producer license—Privileges, requirements, and fees. *Code* 2022:314-55-075. https://apps.leg.wa.gov/wac/default.aspx?cite=314-55-075 [Accessed 9 July 2023].

Ward G, Shakespeare R. *Rendering with radiance: the art and science of lighting visualization*. San Francisco (CA): Morgan Kaufmann Publishers; 1998.

Ward GJ. The RADIANCE Lighting Simulation and Rendering System. In: SIGGRAPH 1994: 21st Annual Conference on Computer Graphics and Interactive Techniques, 1994:459–472.

Xu L, Wei R. Optimal greenhouse lighting scheduling using canopy light distribution model: a simulation study on tomatoes. *Light Res Technol*. 2019:**52**(2):233–246. https://doi.org/10.1177/1477153519825995.